Enhanced spectral resolution in RNA HCP spectra for measurement of $^3J_{C2'P}$ and $^3J_{C4'P}$ couplings and ^{31}P chemical shift changes upon weak alignment

Erin O'Neil-Cabello[a,b], Zhengrong Wu[a], David L. Bryce[a], Edward P. Nikonowicz[b] & Ad Bax[a]

[a]*Laboratory of Chemical Physics, NIDDK, National Institutes of Health, Bethesda, MD 20892-0520, U.S.A.;* [b]*Rice University, Department of Biochemistry and Cell Biology, POB 1892, Houston, TX 77251, U.S.A.*

Abstract

The 'out-and-back' 3D HCP experiment, using gradient- and sensitivity-enhanced detection, provides a convenient method for assignment of the ^{31}P NMR spectra and accurate measurement of the ^{31}P chemical shifts of ribonucleic acids. The ^{13}C resolution in such spectra can be doubled, at the cost of a 50% reduction in sensitivity, by combining ^{13}C evolution during the ^{13}C-$\{^{31}P\}$ de- and rephasing periods. The multiple connectivities observable for a given ^{31}P, including correlations to the intranucleotide $C5'H_2$ and $C4'H$ groups, and the $C2'H$, $C3'H$ and $C4'H$ groups of the preceding nucleotide, permit independent measurements of the ^{31}P shift. The ^{13}C spectrum of these groups is typically crowded for an RNA molecule in isotropic solution and overlap becomes more problematic in media used to achieve partial alignment. However, many of these correlations are resolvable in the combined-evolution HCP spectrum. The difference in ^{31}P chemical shift between isotropic solution and a medium containing liquid crystalline Pf1 provides information on the orientation of phosphate groups. The intensities measured in the 3D HCP spectrum, obtained for an isotropic sample, yield values for the $^3J_{C2'P}$ and $^3J_{C4'P}$ couplings, thereby providing important restraints for the backbone torsion angles ε and β. The experiments are illustrated for a uniformly ^{13}C-enriched, 24-residue stem-loop RNA sequence, and results for the helical stem region show close agreement between observed $\Delta\delta(^{31}P)$ values and those predicted for a model A-form RNA helix when using a uniform ^{31}P CSA tensor. This confirms that $\Delta\delta(^{31}P)$ values can be used directly as restraints in refining nucleic acid structures.

Introduction

NMR spectroscopy provides a convenient method for studying the structure and dynamics of RNA oligonucleotides as large as 25 kD (Wu et al., 2001a; Cabello-Villegas et al., 2002; Lawrence et al., 2003; Leeper et al., 2003; Lukavsky et al., 2003). Traditionally, many of the structural restraints have relied on quantitative interpretation of ^1H-^1H NOEs, supplemented by $^3J_{HH}$ and $^3J_{HP}$ couplings. However, with the introduction of isotopic enrichment procedures for RNA and DNA (Batey et al., 1992; Nikonowicz et al., 1992; Ono et al., 1994; Farmer et al., 1995; Zimmer and Crothers, 1995; Masse et al., 1998), a number of new restraints are now available. In par-

ticular, ^{13}C enrichment permits measurement of the χ-angle related couplings between H1$'$ and C6/C8 (Ippel et al., 1996; Trantirek et al., 2002), and the three-bond ^{13}C-^{31}P J couplings, which report on the ε and β torsion angles (Legault et al., 1995; Richter et al., 1998). Experimental information regarding the backbone torsion angles also can be derived from quantitative interpretation of relaxation interference (cross correlations) effects (Richter et al., 2000). With ^{15}N enrichment, identification of internucleotide hydrogen bonding partners has become readily possible by detection of $^hJ_{NN}$ couplings (Dingley and Grzesiek, 1998). Several recent reviews provide excellent overviews of these methods and their application towards RNA structural studies (Marino et al., 1999; Allen

et al., 2001; Perez-Canadillas and Varani, 2001; Zidek et al., 2001; Furtig et al., 2003).

All of the above mentioned NMR parameters provide local structural information, either in terms of torsion angles or in terms of interproton distance or hydrogen bonding partner. Introduction of weak alignment, usually by means of a dilute liquid crystal-line suspension (Tjandra and Bax, 1997; Clore et al., 1998; Hansen et al., 1998), or by using an anisotrop-ically compressed hydrogel (Sass et al., 2000; Tycko et al., 2000; Kim et al., 2002), permits the facile measurement of internuclear dipolar couplings. These complement the traditional restraints by providing global information on the orientation of internuclear vectors relative to a single axis system, that of the molecular alignment tensor. Even when relatively few such dipolar couplings are measured, considerably improved definition of the global structure has been demonstrated (Bayer et al., 1999; Mollova et al., 2000; Sibille et al., 2001; Warren and Moore, 2001). When many dipolar couplings are measured, including ^{1}H-^{1}H couplings, they can accurately define the structure of DNA oligomers, even in the absence of NOEs (Wu et al., 2003). We are currently engaged in an effort to evaluate which orientational restraints are most easily measured in RNA oligomers, and whether this inform-ation is sufficient for defining the 3D structure of such molecules. Although the spectral dispersion of RNA is typically considerably less favorable compared to DNA, we recently have shown that as many as five dipolar couplings can be measured from a single H1$'$-C1$'$-C2$'$ 3D cross peak (O'Neil-Cabello et al., 2004), and that even the H5$'$-H5$''$ and heteronuclear C5$'$-H$_2$ dipolar couplings can be measured for every ribose in a 24-nucleotide stem-loop molecule (Miclet et al., 2003).

Here, we demonstrate that restraints regarding the phosphodiester backbone conformation can be ob-tained from 'out-and-back' HCP spectra (Heus et al., 1994; Legault et al., 1995; Richter et al., 1998). We demonstrate that by combining ^{13}C evolution during both the ^{13}C-{^{31}P} de- and rephasing periods, very high resolution can be obtained, sufficient to resolve the vast majority of the correlations, even in the helical stem region of a 24-nucleotide stem-loop structure.

Experimental section

Two samples, each containing 1.9 mM of a uniformly ^{13}C-enriched RNA oligomer, derived from helix-35 of

E. coli 23S ribosomal RNA, and modified to contain pseudouridine at position 746 (inset, Figure 2), were prepared in thin-wall Shigemi microcells (270 μl). As a result of the procedure used to generate the oligomer, it lacked ^{13}C enrichment for the 5$'$-terminal nucle-otide, G737. Both samples were extensively dialyzed against the same buffer, containing 10 mM NaCl, 10 mM potassium phosphate, 0.02 mM EDTA in 99% D$_2$O, pH 6.8 (direct meter reading in D$_2$O). One of the two samples additionally contained 22 mg/ml Pf1, which serves as the liquid crystalline alignment medium (Hansen et al., 1998).

3D HCP NMR spectra were recorded at 600 MHz on a Bruker DMX600 spectrometer, equipped with a quadruple resonance PFG probehead. ^{13}C-{^{31}P} de- and rephasing periods were 25 ms each, with the rephasing period also serving as the ^{13}C shift encoding F$_2$ dimension of the experiment. Gradient-and-sensitivity-enhanced conversion (Kay et al., 1992) from ^{13}C to ^{1}H was used. Acquisition times were 48 ms in the ^{31}P dimension, 50 ms in the ^{13}C di-mension, and 85 ms in the ^{1}H dimension. The total acquisition time was 40 h per 3D spectrum, and 1 h per 2D reference spectrum.

For calculating the difference in ^{31}P chemical shift between aligned and isotropic spectra, it is necessary to account for the change in carrier frequency associ-ated with the ^{2}H lock resonance being split as a result of the residual quadrupole coupling, qcc. In principle, depending on whether the spectrometer is locked on the downfield or upfield doublet component, this res-ults in an upfield or downfield offset of $\gamma_X qcc/2\gamma_D$ Hz, where γ_X is the gyromagnetic ratio of nucleus X. However, small deviations from this expected off-set, resulting from unspecified experimental problems, have previously been noted (Choy et al., 2001). In our experiments, after correction for the change in field caused by the lock splitting (qcc = 19.2 Hz), the chemical shift change observed for the residual HDO resonance was less than 1 ppb, and chemical shift changes for ribose ^{1}H resonances fell into the ±4 ppb range, as expected for ^{1}H nuclei with relat-ively small CSA. Moreover, a plot of calculated versus observed $\Delta\delta(^{31}$P) did not reveal any systematic dif-ference, which would have occurred if the $\gamma_P qcc/2\gamma_D$ correction were inadequate.

A detailed discussion of determination of the alignment tensor magnitude and orientation has been presented previously (Bryce and Bax, 2004). Here, we use the alignment tensor, obtained previously by fitting the $^1D_{CH}$ $^1D_{CC}$, $^2D_{CH}$, $^3D_{HH}$ couplings (see Support-
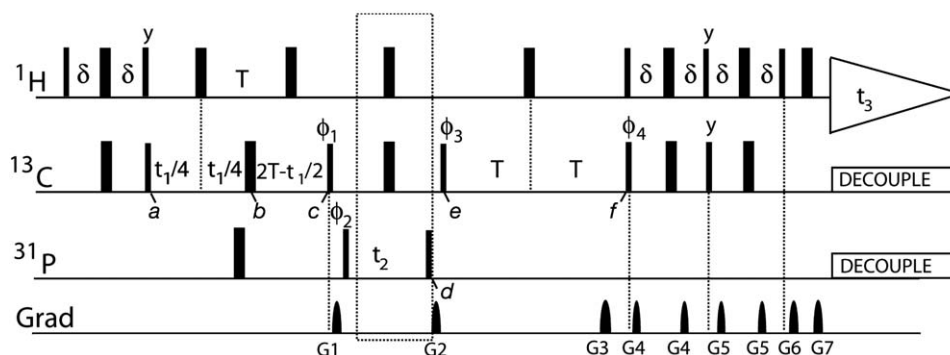
Figure 1. Pulse sequence of the combined-evolution 3D CECT-HCP experiment. Narrow and wide pulses correspond to 90° and 180°, respectively. Unless marked, pulse phases are x. Delay durations: T = 12.5 ms, δ = 1.55 ms. Phase cycling for the 3D version: ϕ_1 = x,y; ϕ_2 = 4(x),4(−x); ϕ_3 = −x,y,x,−y; ϕ_4 = −x; Receiver = 2(x),4(−x),2(x). Quadrature in the t_2 dimension is obtained in the regular States-TPPI manner; quadrature in the t_1 dimension is obtained in the regular Rance–Kay mode (Kay et al., 1992), by inverting the polarity of the encoding gradient G3 and phase ϕ_4. For the 2D reference experiment, the pulse sequence segment in the dotted box, including the t_2 evolution period, is eliminated, and phase cycling is as above, except for the receiver = 2(x),2(−x). Pulsed field gradients: G1,2,3,4,5,6,7 = 2, 2, 4.01, 0.5, 0.5, 0.7, 0.307 ms. Directions: (−x,y), (x,y,z), (−x,−y,−z), x, y, (x,y,z), (−x,−y,−z). All gradients are sine-bell shaped, with combined (x/y/z) gradient peak amplitudes of 20, 10, 22, 25, 25, 22, 22 G/cm. The ^{13}C 90_{ϕ_1},180, 90_{ϕ_3} pulses, with the above phase cycle, simulate the effect of a 180° pulse, and the phase of transverse ^{13}C magnetization just after the 90_{ϕ_3} pulse (after all steps of the phase cycle are combined) is opposite to that just prior to the 90_{ϕ_1} pulse, but its magnitude is halved.

ing information of O'Neil-Cabello et al. (2004)) in the stem region of the oligonucleotide (nucleotides G738-A743; U754-C759; total 94 couplings) to the corresponding ribose vectors in the high-resolution (1.2-Å) X-ray structure of an averaged A-form duplex structure (PDB entry 1QCU (Klosterman et al., 1999)). The fit yields $D_a^{CH} = -20.6 \pm 0.5$ Hz; $R = 0.31 \pm 0.03$; Euler angles relative to 1QCU of α = 12.6 ± 0.6°, β = −16.5 ± 1.5°, and γ = 1.1 ± 1.3°. Note that due to the different nucleotide sequence of the X-ray structure relative to the sequence studied here, primarily ribose RDCs (90 total), and only four $^1D_{CH}$ base couplings, could be used in the SVD fitting procedure.

Results and discussion

Combined evolution HCP

Implementation of the combined evolution concept in the constant-time HCP experiment, below referred to as CECT-HCP, differs slightly from its original implementation (Madsen and Sorensen, 1992; McCoy, 1998). Therefore, prior to describing application of the CECT-HCP method to RNA, we briefly describe the pulse sequence with emphasis on its combined-evolution aspect. The pulse scheme itself (Figure 1) is nearly identical to the scheme used by Heus et al. (Heus et al., 1994), but differs by (a) use of the popular gradient-enhanced detection scheme (Kay et al.,

1992), (b) the slightly different way ^{1}H decoupling is accomplished during ^{13}C evolution, (c) the phase cycling and (d) the distance over which the 180° ^{13}C pulse, applied at time point *b*, is moved. This last point is related to the combined evolution aspect and will be described below. For simplicity, we will ignore the effect of the ^{1}H spin state and ^{1}H-^{13}C J coupling, which can be added in the standard manner, and we consider coupling of ^{13}C to only a single ^{31}P nucleus, with 2T = 1/(2J$_{CP}$).

In the standard experiment, the ^{13}C 180° pulse applied at time *b* starts at the midpoint between time points *a* and *c*, such that for the first t_1 increment the ^{13}C magnetization is refocused at time *c*. In subsequent t_1 increments, it is stepwise moved to the right, until at the end of the CT evolution period (for a maximum t_1 duration of 2T) it meets up with the 90_{ϕ_1} pulse. This corresponds to a total evolution time equal to 2T, *i.e.*, the total duration between time points *a* and *c*. Depending on the phase ϕ_1, either the sine or cosine component of the ^{13}C magnetization, antiphase with respect to ^{31}P, is converted into 2C$_z$P$_z$ two-spin order, prior to evolving as transverse ^{31}P magnetization during t_2, back conversion to 2C$_z$P$_z$ at time *d*, and ^{13}C-{^{31}P} rephasing between time points *e* and *f* (without ^{13}C chemical shift evolution, due to a 180° ^{13}C pulse applied at the mid-point between points *e* and *f* in the regular HCP experiment) (Heus et al., 1994).
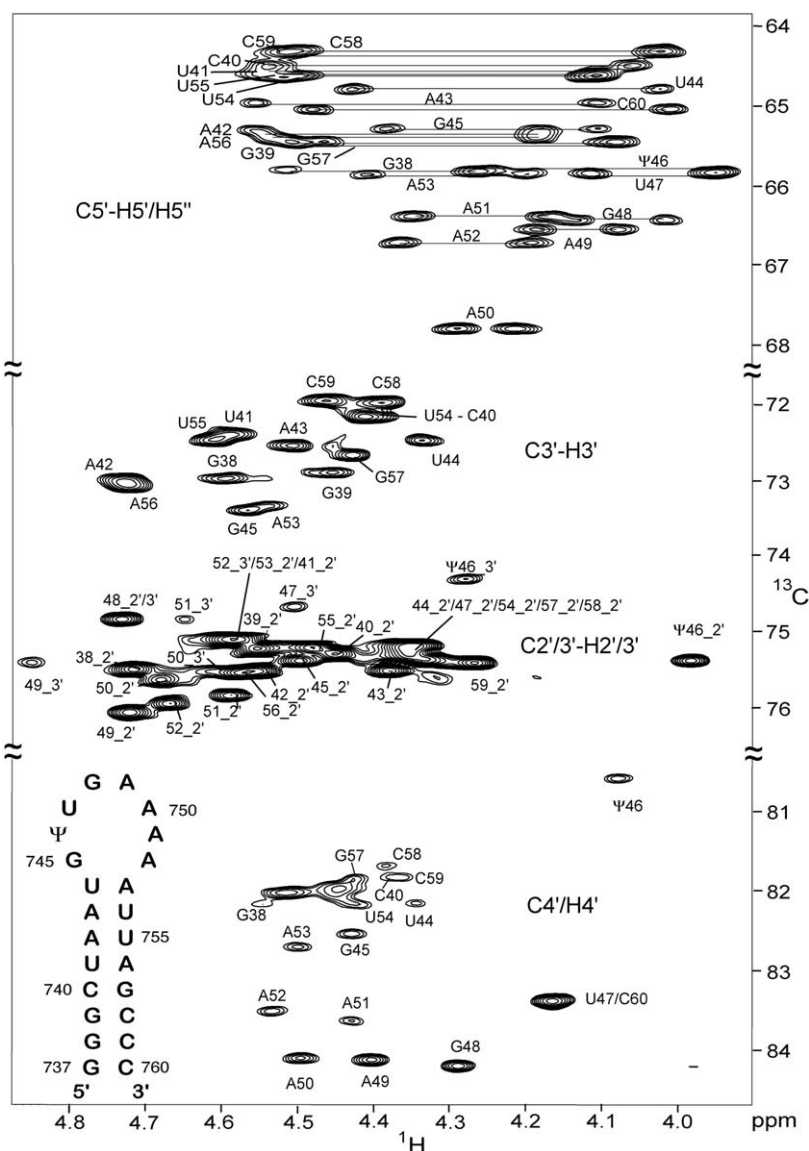
Figure 2. ^{1}H-^{13}C cross section through the 600 MHz pseudo-3D HCP reference spectrum of the RNA stem-loop sequence shown in the inset, taken at zero frequency in the ^{31}P dimension. Except for the absolute values of the peak intensities, the cross section is identical to that of the 2D ^{13}C-^{1}H correlation used to create it. The combined-evolution constant-time 2D ^{13}C-^{1}H reference spectrum was generated with the pulse sequence of Figure 1, using a 166* × 512* data matrix, with spectral windows of 22.1 ppm (^{13}C) and 10 ppm (^{1}H). Correlations are identified by the last 2 digits of the 23S rRNA residue number.

In the CECT-HCP experiment, the 180° ^{13}C pulse at time point b initially ($t_1 = 0$) is adjacent to the 90° pulse at time point a. ^{13}C magnetization then evolves for time 2T, and accumulates a transverse phase $2\Omega_C T$. So, just prior to time point c, the transverse ^{13}C magnetization of interest is described by $2\sin(2\Omega_C T)C_y P_z + 2\cos(2\Omega_C T)C_x P_z$. For $\phi_1 = x$, the $\sin(2\Omega_C T)$ component is transferred to two-spin order ($C_z P_z$) at time c. After ^{31}P evolution and ignoring

transverse ^{31}P relaxation, a fraction $-\cos(\Omega_P t_2)$ of this magnetization is converted back into $C_z P_z$ two-spin order at time d, prior to being converted into $-2\sin(2\Omega_C T)\cos(\Omega_P t_2)C_y P_z$ by the $90_{\phi 3}$ pulse ($\phi_3 = -x$) at time point e. In the second scan, $\phi_1 = y$ and $\phi_3 = y$, yielding $2\cos(2\Omega_C T)\cos(\Omega_P t_2)C_x P_z$ immediately after the $90_{\phi 3}(^{13}C)$ pulse. As the remainder of the pulse sequence (after time point e) is the same in the first two scans of the experiment, the signals of the

first two scans can be added directly at time point e, yielding $-2\sin(2\Omega_C T)C_y P_z + 2\cos(2\Omega_C T)C_x P_z$. This corresponds to a transverse ^{13}C signal with a phase exactly opposite to that noted above just prior to time point c. Therefore, after additional transverse evolution for time 2T, at time f, the ^{13}C shift evolution has fully refocused, as required for $t_1 = 0$. At this point the magnetization is transferred to ^{1}H using the regular Rance–Kay pulse sequence element (Kay et al., 1992).

Applying the same reasoning as above, it is clear that the combined magnetization of transients 1 and 2 at time point e corresponds to a ^{13}C signal that has evolved for a time $-2T + t_1$. Subsequent transverse ^{13}C evolution between time points e and f for a fixed duration of 2T results in total transverse evolution of t_1, with $t_{1,max} = 4T$. For the present case, where $2T = 1/J_{CC} = 25$ ms, this corresponds to a maximum combined t_1 evolution of 50 ms.

After co-addition of the signals from transients 1 and 2, above, the phase of the ^{13}C magnetization at time point e is inverted relative to that just prior to time point c, as if a 180_x pulse had been applied to it. However, it should be noted that two transients were used to generate this transverse signal, each with independent noise. Therefore, the noise in this summed signal is higher by $\sqrt{2}$. In addition, it takes two transients to generate this signal compared to the case where a $180°$ pulse is used, leading to another $\sqrt{2}$ loss in sensitivity per unit of measuring time. So, the total S/N-loss resulting from this procedure is a factor 2. Relative to the original HCP experiments, this 2-fold loss in S/N is partially compensated by the $\sqrt{2}$ gain resulting from the Rance–Kay procedure. However, if the original HCP experiment is conducted with the Rance–Kay transfer (while shifting the ^{13}C evolution period between the ^{31}P evolution period and ^{1}H detection), this same gain can be obtained in the regular HCP experiment. Therefore, the price paid for combined evolution is a two-fold loss in S/N per unit of measuring time. The two-fold higher ^{13}C resolution, obtained from the CECT-HCP experiment over the regular CT-HCP experiment, frequently is key to resolving the correlations of interest, in particular in the crowded H4′-C4′ region of the RNA spectrum for which the intensity of 3D HCP correlations tends to be high. As the total time during which the spin system relaxes is the same for both the regular and CECT-HCP experiments, relative intensities of correlations in the two types of 3D spectra remain the same. In our experience, this tends to be an advantageous feature of the CECT-HCP over the regular HCP experiment, recorded with a two-fold longer CT period.

Reference spectrum for quantitative J correlation

The 2D reference spectrum is acquired with the same CECT-HCP pulse sequence as the 3D spectrum, but only the first ^{1}H-^{13}C plane is recorded, with the phase cycling altered such that magnetization that does not get transferred to ^{31}P is selected (Richter et al., 1998) (see legend to Figure 1). To first order, this magnetization therefore is subject to the same relaxation losses as the magnetization which does get transferred to ^{31}P, and is attenuated to the same extent during the ^{13}C-$\{^{31}$P$\}$ de/rephasing periods, where ^{13}C magnetization is transverse.

Although intensities in a 3D spectrum can be compared directly against those in a 2D reference spectrum, which is necessary to extract the size of the coupling through the principle of quantitative J correlation (Bax et al., 1994), the scaling factors involved in such comparisons can sometimes be confusing. Therefore, the 2D spectrum was converted into a pseudo-3D spectrum, by first appending a file of the same size containing all zeroes, to represent the imaginary component of the complex '^{31}P dimension'. This combined file then was appended 19 times to the original 2D data set (to represent the same 20 complex sampling points used in the 3D spectrum), resulting in zero modulation frequency in the ^{31}P dimension. Exponential line broadening of 13 Hz was then used to mimic the T_2 decay observed in the true 3D HCP spectrum, and both the true and pseudo-3D spectra were subsequently processed identically, using NMR-Pipe software (Delaglio et al., 1995). In principle, differences in the ^{31}P line widths from site to site will affect the ratio of the peak heights (but not the volumes) in the reference and true HCP spectra. In practice the variations in ^{31}P line width in the 3D spectrum were found to be small ($< \pm15\%$) and simple peak heights were therefore used in all calculations, avoiding volume integration problems in cases where peak separation does not reach the baseline.

The intensity ratio for a 3D HCP correlation and its pseudo-3D reference intensity is given by (Richter et al., 1998):

$$I/I_{ref} = \sin^2(2\pi J_{CP}T)/\cos^2(2\pi J_{CP}T), \tag{1}$$

where 2T is the 25 ms ^{13}C-$\{^{31}$P$\}$ de/rephasing duration, and J_{CP} represents the two- or three-bond J_{CP} coupling giving rise to the 3D cross peak.

Application to helix-35 of E. coli *23S ribosomal RNA*

When the method is applied to helix-35 of *E. coli* 23S ribosomal RNA, overlap remains a problem in the 2D (or pseudo-3D) reference spectrum (Figure 2), despite the high ^{13}C resolution. The remaining resonance overlap occurs primarily in the C4' region. However, as the location of the C4'-H4' correlation is known precisely from the resolved 3D spectrum, the intensity at the corresponding location in the reference spectrum is used as an upper limit for the reference intensity for those peaks that are unresolved. Thus, for cases where the 3D HCP correlation is resolved, this results in a lower limit for the $^3J_{CP}$ coupling of interest (Table 1). For the loop residues, which are of particular interest as their conformation is unknown, most of the reference peaks are well resolved, allowing their intensity to be measured directly.

Figure 3 shows an overlay of two ^{13}C-^{31}P cross sections through the 3D HCP spectra, recorded under isotropic conditions and in Pf1. Small changes in chemical shift result from incomplete averaging of the ^{31}P and ^{13}C CSA tensors in the Pf1 medium (see below). Even though many of the corresponding ^{13}C-^{1}H correlations in the 2D spectrum of Figure 1 partially overlap, most of the 3D correlations in the 3D HCP spectrum are well resolved. For the helical stem region, no correlation to C2' is observed for any of the nucleotides, which puts very useful upper limits of 1.5 Hz on the value of $^3J_{C2'P}$. Using the Karplus equation for $^3J_{C2'P}$ (Mooren et al., 1994):

$$^3J_{CP} = 8.0\cos^2\theta - 3.4\cos\theta + 0.5 \qquad (2)$$

such a small $^3J_{C2'P}$ value is only compatible with $\varepsilon = -164 \pm 25°$ or $\varepsilon = 44 \pm 25°$. The absence of any $^3J_{C2'P}$ values larger than 2.8 Hz indicates that the gauche- conformer of ε is not significantly populated for any of the phosphodiesters in the sequence. As previously noted (Legault et al., 1995; Murray et al., 2003), the $\varepsilon = 44°$ region (gauche+) is energetically unfavorable and therefore can also be excluded. This is confirmed by large $^3J_{C4'iPi+1}$ values (>5 Hz; Table 1) for all but two of the phosphodiesters, indicative of trans arrangements, $\varepsilon = 180 \pm 60°$. For the vast majority of $J_{C4'iPi}$ couplings, relatively large values also point to a near-trans arrangement about the β angle ($\beta = 180 \pm 50°$). Remarkably, in the loop region (G745-A752), we find $^3J_{C4'iPi} > {}^3J_{C4'iPi+1}$, suggesting that β retains its near-trans geometry, found in a regular A-form helix, more closely than ε.

$^2J_{C3'Pi+1}$ and $^2J_{C5'Pi}$ couplings could also be measured for the majority of nucleotides (Table 1), but no clear structural interpretation is available for these couplings. Very little variation is observed for the $^2J_{C5'Pi}$ couplings. For the six nucleotides where $^2J_{C5'Pi}$ could be measured twice, through both H5' and H5″, the pairwise rms difference between the measurements was small (0.26 Hz), indicative of random errors ≤0.2 Hz in their individual measurements. Systematic sources of error, related to pulse imperfection or deviations from the assumption of a uniform 13 Hz ^{31}P line width, could affect both derived couplings by the same amount, and are estimated not to exceed ±10%.

An overlay of corresponding ^{31}P/^{13}C cross sections through the 3D HCP spectra taken in the isotropic and aligned states shows that chemical shift differences between the isotropic and aligned states can be measured reliably (Figure 3). Since most ^{31}P resonances display resolved correlations to multiple ribose carbons, independent measurements of many of the $\Delta\delta(^{31}P)$ values are available. Although the reported $\Delta\delta(^{31}P)$ values correspond to the best resolved and/or most intense correlation, agreement between $\Delta\delta(^{31}P)$ values for any given site where multiple measurements were available was excellent, indicating experimental errors of less than ±3 ppb for most of the ^{31}P resonances. The range of observed $\Delta\delta(^{31}P)$ values covers −40 to +64 ppb (Table 1). As described previously (Lipsitz and Tjandra, 2001; Wu et al., 2001b), these $\Delta\delta(^{31}P)$ values are readily incorporated into structure calculations. Changes in ^{13}C chemical shift are also easily measured, but in the absence of accurate knowledge regarding the ribose ^{13}C CSA tensor magnitude and orientation specific to RNA in solution, these data are not yet usable in structure calculations.

For the magnitude of the ^{31}P CSA tensor values, we use rounded values previously measured by solid state NMR for phosphodiester compounds (barium diethylphosphate and various phospholipids) (Herzfeld et al., 1978). These rounded principal components of the traceless part of the ^{31}P CS tensor ($\delta_{11} = 80$ ppm; $\delta_{22} = -20$ ppm; $\delta_{33} = -100$ ppm; δ_{11} is orthogonal to the O1P-P-O2P plane and δ_{22} bisects the O1P-P-O2P angle) previously have been shown to agree well with $\Delta\delta(^{31}P)$ values measured in DNA (Lipsitz and Tjandra, 2001; Wu et al., 2001b). Note that δ refers to the chemical shift anisotropy, not to the oppositely signed magnetic shielding, and does not include the isotropic shift contribution, which does not affect $\Delta\delta(^{31}P)$ values measured in our experiment. Using an alignment tensor derived as described in the Experi-

Table 1. J$_{CP}$ couplings, ^{31}P isotropic chemical shifts, and differences in chemical shifts between aligned and isotropic forms of an RNA stem-loop

Nucleotide	^{3}J(C2$'_i$-P$_{i+1}$) (Hz)	^{2}J(C3$'_i$-P$_{i+1}$) (Hz)	^{3}J(C4$'_i$-P$_{i+1}$) (Hz)	^{3}J(C4$'_i$-P$_i$) (Hz)	^{2}J(C5$'_i$-P$_i$) (Hz)	δ(^{31}P)[d] (ppm)	$\Delta\delta$(^{31}P)[f] (ppb)
G738	≤1.4[a]	4.6	9.6	8.0	4.1	−3.57	−40
G739	≤1.2[a]	4.9	≥7.0[b]	≥7.2[b]	≥3.7[b]	−3.75	31
C740	≤1.2[a]	c	c	≥8.0[b]	4.4	−4.32	43
U741	≤1.2[a]	5.4	c	c	≥4.0[b]	−4.09	e
A742	≤1.2[a]	5.0	≥8.0[b]	c	≥4.5[b]	−3.84	28
A743	≤1.2[a]	4.4	c	≥9.4[b]	5.1	−4.10	28
U744	≤1.5[a]	3.6	7.3	8.1	5.0	−4.15	45
G745	1.7	5.2	6.7	8.6	4.8	−3.96	55
Ψ746	2.4	5.8	6.3	8.1	c	−3.58	23
U747	2.6	4.3	≥5.0[b]	≥7.6[b]	4.9	−3.95	6
G748	c	c	4.0	8.2	4.3	−3.08	−22
A749	2.8	3.3	5.3	8.0	5.0	−3.36	9
A750	2.4	≥2.9[b]	4.9	7.5	4.8	−3.85	21
A751	2.8	4.4	5.0	7.8	4.9	−3.94	6
A752	2.5	≥2.4[b]	4.6	7.5	4.7	−3.58	−21
A753	≤1.7[a]	≥3.7[b]	7.5	7.2	4.5	−3.86	7
U754	≤1.5[a]	c	≥8.6[b]	≥8.3[b]	≥3.5[b]	−4.24	49
U755	≤1.2[a]	5.4	≥8.3[b]	c	4.4	−4.13	64
A756	≤1.5[a]	5.5	≥7.1[b]	≥8.7[b]	≥4.6[b]	−3.86	46
G757	≤1.4[a]	3.7	≥8.5[b]	≥8.6[b]	≥3.8[b]	−4.01	23
C758	≤1.7[a]	3.3	8.4	7.8	≥4.2[b]	−4.48	−4
C759	≤1.1[a]	5.0	8.5	8.5	≥3.5[b]	−4.29	5
C760				≥7.9[b]	5.0	−4.16	13

[a]Upper limit for coupling based on the absence of a 3D correlation at the noise level.
[b]Lower limit for coupling, using overlapping intensity in reference spectrum.
[c]Not determined due to overlap in both the reference and the 3D spectrum.
[d]Indirectly referenced to hypothetical internal (CH$_3$O)$_3$PO (Markley et al., 1998).
[e]Insufficiently resolved for accurate measurement.
[f]$\Delta\delta = \delta_{obs}$ (aligned) $- \delta_{obs}$ (isotropic)

mental section, $\Delta\delta$(^{31}P) values can be predicted for the helical stem region.

The correlation between observed and predicted values is very good (Figure 4), particularly considering that $\Delta\delta$(^{31}P) values for this alignment tensor cover only a fraction of the range (-95 to $+85$ ppb) expected if the phosphate orientations were uniformly distributed relative to the alignment tensor. In the helical stem region of the structure, the range of observed $\Delta\delta$(^{31}P) values is only 68 ppb, resulting in the relatively low correlation coefficient seen in Figure 4 ($R_P = 0.96$). However, the quality factor, $Q = 0.15$, indicates very close agreement between the $\Delta\delta$(^{31}P) values and the helical model structure, comparable to what is typically seen when comparing backbone dipolar couplings with corresponding protein X-ray structures in the 1–1.5Å resolution range.

It is worth noting that no adjustable parameters were used to generate Figure 4; the alignment tensor obtained from dipolar couplings was simply used to calculate the $\Delta\delta$(^{31}P) values expected for 1QCU, using the rounded ^{31}P CSA values discussed above (Lipsitz and Tjandra, 2001; Wu et al., 2001b). Note that changes in alignment tensor rhombicity by more than three standard deviations from the values obtained from the fit (Experimental Section) do not significantly impact the quality of the correlation (Supporting Information). Any uncertainty in the alignment tensor magnitude only affects the slope of the correlation, which is already very close to optimal. Using CSA values specific to barium diethylphosphate (Herzfeld et al. 1978) instead of the rounded numbers discussed above also has a negligible impact on the quality of the correlation (Supporting Information).
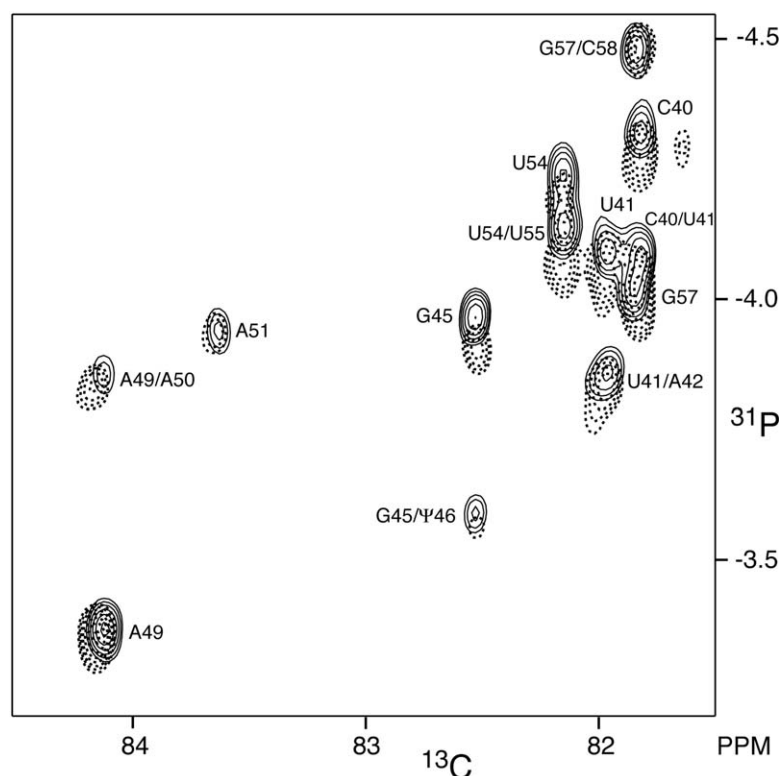
Figure 3. Overlay of the C4′ region of a ^{13}C-^{31}P cross section taken through the combined evolution 3D HCP spectra at a ^{1}H frequency of 4.41 ppm. Solid contours correspond to the isotropic RNA sample, dashed contours to the sample in Pf1. Small differences in peak position in the ^{31}P and ^{13}C dimensions result from incomplete averaging of ^{31}P and ^{13}C chemical shift anisotropy, respectively. The spectrum results from a 166* × 20* × 512* data matrix, with spectral windows of 22.1 ppm (^{13}C), 1.7 ppm (^{31}P), and 10 ppm (^{1}H). Correlations are labeled as in Figure 2. ^{31}P shifts are relative to trimethyl phosphate; ^{13}C shifts are relative to DSS.

Notwithstanding the close agreement between observed and predicted $\Delta\delta(^{31}$P) values seen in Figure 4, the rmsd (6.5 ppb) considerably exceeds the measurement error, estimated at ≤ 3 ppb based on reproducibility in cases where multiple correlations are available to measure the same $\Delta\delta(^{31}$P). This increased rmsd presumably reflects small, sequence-specific variations in the precise geometry surrounding each phosphate group. It is these variations that we believe to be largely responsible for the small differences in isotropic ^{31}P shifts and $^3J_{CP}$ couplings observed within the stem region. The observation that the difference between observed and predicted values exceeds the measurement error suggests that structure refinement by inclusion of $\Delta\delta(^{31}$P) values as experimental restraints can improve the geometry over that of the model helix. However, although we have no experimental indication for this, if site-to-site variations in the applicable individual ^{31}P CSA tensor magnitude, rhombicity or orientation were relatively large, this

could also be responsible for the rmsd being larger than the measurement error, as could a relatively high degree of uniform, anisotropic motion of the phosphodiester linkages, or differences in the true orientation of the ^{31}P CSA tensor from those assumed in the present study.

Concluding remarks

Combined evolution during both de- and rephasing periods of the constant-time HCP experiment yields a two-fold increase in spectral resolution. This is particularly important in the analysis of medium-sized RNA oligomers, where spectral overlap in the regular CT-HCP experiment severely limited the number of structurally valuable $^3J_{CP}$ values extractable from the spectrum. These data, which yield restraints for the β and ε torsion angles, are obtained at no additional cost from the isotropic HCP spectrum, when using the HCP experiment to measure $\Delta\delta(^{31}$P) values between

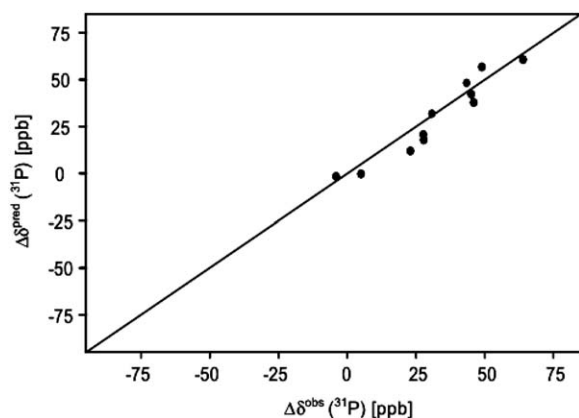*Figure 4.* Correlation between observed and predicted $\Delta\delta(^{31}P)$ values for the helical stem residues of the stem-loop structure depicted in Figure 2. Predicted values were obtained by first best-fitting the experimental dipolar couplings of the helical stem region to a 6-basepair fragment of the high resolution X-ray structure of an A-form helical RNA fragment (PDB code 1QCU) (see Experimental Section) and then, for the alignment tensor obtained in this manner, calculating the predicted $\Delta\delta(^{31}P)$ values using the procedure described by Wu et al. (2001). Estimated measurement uncertainty in $\Delta\delta(^{31}P)$ is ± 3 ppb; the rmsd between observed and predicted values is 6.5 ppb. Pearson's correlation coefficient, $R_P = 0.96$.

isotropic and aligned states. The J coupling information provides a critical complement to the $\Delta\delta(^{31}P)$ restraints, because in the absence of β and ε torsion angle restraints the $\Delta\delta(^{31}P)$ value potentially can be satisfied for multiple, very different orientations of the phosphate group. For example, the orientation of the phosphate group relative to the alignment tensor generally will differ significantly for BI and BII conformations of the phosphodiester linkage, and $\Delta\delta(^{31}P)$ together with the $^3J_{CP}$ couplings can distinguish these conformers. Also, turns of the phosphate backbone can be enabled by non-standard values of torsional angles α and ζ (Shi and Moore, 2000) that are not manifest through β and ε. Thus, $\Delta\delta(^{31}P)$ offers a powerful tool to quantitatively characterize the phosphate backbone conformation when coupled with an accurate complement of J-derived restraints.

In principle, the change in ^{13}C-^{31}P couplings between isotropic and aligned states provides dipolar coupling information, but these couplings are nearly two orders of magnitude smaller than $^1D_{CH}$ couplings, and in practice the error in their measurement ($\sim$0.3–0.5 Hz) is comparable to the size of these couplings. Their measurement was therefore not pursued.

The old idea (Madsen and Sorensen, 1992; McCoy, 1998) to double the ^{13}C resolution by utilizing both the ^{13}C-^{31}P de- and rephasing periods for ^{13}C

chemical shift encoding was key to resolving many of the resonances. This type of combined evolution has been used relatively little, but it is directly applicable to most of the protein and nucleic acid 3D experiments, particularly those of the 'out-and-back' type that involve ^{13}C constant-time dephasing and rephasing intervals. The two-fold loss in sensitivity inherent to combining two such CT intervals, when multiple quantum approaches are not feasible, is often preferred over doubling the duration of the regular CT evolution period, which can result in larger sensitivity losses. Moreover, when combining evolution from separate CT periods, the relative intensities remain identical to those in the standard mode of such experiments. Therefore, this approach is particularly useful in cases where limited exchange broadening is present, and where doubling a CT evolution duration is impractical, as applies to many RNA structures. Conceptually, combined-evolution experiments are also very similar to reduced dimensionality (RD) experiments (Szyperski et al., 1993; Simorre et al., 1994), where in the present case the two evolutions that are combined correspond to the same nucleus. Considering that the two evolving frequencies are identical, only their sum carries useful information and is selected by the phase cycle, whereas in RD both the sum and the difference of the two evolving frequencies are of interest.

Acknowledgements

Supporting Information Available: Two figures displaying (a) the effect of changing alignment tensor rhombicity by $\pm$ 0.1 from the value used to generate Figure 4, and (b) the correlation diagram of Figure 4 when using the ^{31}P CSA values previously reported for barium diethyl phosphate. This material is available in the electronic edition of the journal at: http//kluweronline.com/issn/0925-2738.

References

Allen, M., Varani, L. and Varani, G. (2001) In *Nuclear Magnetic Resonance of Biological Macromolecules*, Pt B, pp. 357–376.

Batey, R.T., Inada, M., Kujawinski, E., Puglisi, J.D. and Williamson, J.R. (1992) *Nucl. Acids Res.*, **20**, 4515–4523.

Bax, A., Vuister, G.W., Grzesiek, S., Delaglio, F., Wang, A.C., Tschudin, R. and Zhu, G. (1994) In *Nuclear Magnetic Resonance*, Pt C, Oppenheimer, N.J. and James, T.L. (Eds.), pp. 79–105.

Bayer, P., Varani, L. and Varani, G. (1999) *J. Biomol. NMR*, **14**, 149–155.

Bryce, D.L. and Bax, A. (2004) *J. Biomol. NMR*, **28**, 273–287.

Cabello-Villegas, J., Winkler, M.E. and Nikonowicz, E.P. (2002) *J. Mol. Biol.*, **319**, 1015–1034.

Choy, W.Y., Tollinger, M., Mueller, G.A. and Kay, L.E. (2001) *J. Biomol. NMR*, **21**, 31–40.

Clore, G.M., Starich, M.R. and Gronenborn, A.M. (1998) *J. Am. Chem. Soc.*, **120**, 10571–10572.

Delaglio, F., Grzesiek, S., Vuister, G.W., Zhu, G., Pfeifer, J. and Bax, A. (1995) *J. Biomol. NMR*, **6**, 277–293.

Dingley, A.J. and Grzesiek, S. (1998) *J. Am. Chem. Soc.*, **120**, 8293–8297.

Furtig, B., Richter, C., Wohnert, J. and Schwalbe, H. (2003) *Chembiochem.*, **4**, 936–962.

Hansen, M.R., Mueller, L. and Pardi, A. (1998) *Nat. Struct. Biol.*, **5**, 1065–1074.

Herzfeld, J., Griffin, R.G. and Haberkorn, R.A. (1978) *Biochemistry*, **17**, 2711–2718.

Heus, H.A., Wijmenga, S.S., van de Ven, F.J.M. and Hilbers, C.W. (1994) *J. Am. Chem. Soc.*, **116**, 4983–4984.

Ippel, J.H., Wijmenga, S.S., deJong, R., Heus, H.A., Hilbers, C.W., deVroom, E., vanderMarel, G.A. and vanBoom, J.H. (1996) *Magn. Reson. Chem.*, **34**, S156–S176.

Kay, L.E., Keifer, P. and Saarinen, T. (1992) *J. Am. Chem. Soc.*, **114**, 10663–10665.

Kim, I., Lukavsky, P.J. and Puglisi, J.D. (2002) *J. Am. Chem. Soc.*, **124**, 9338–9339.

Klosterman, P.S., Shah, S.A. and Steitz, T.A. (1999) *Biochemistry*, **38**, 14784–14792.

Lawrence, D.C., Stover, C.C., Noznitsky, J., Wu, Z.R. and Summers, M.F. (2003) *J. Mol. Biol.*, **326**, 529–542.

Leeper, T., Leulliot, N. and Varani, G. (2003) *Nucl. Acids Res.*, **31**, 2614–2621.

Legault, P., Jucker, F.M. and Pardi, A. (1995) *FEBS Lett.*, **362**, 156–160.

Lipsitz, R.S. and Tjandra, N. (2001) *J. Am. Chem. Soc.*, **123**, 11065–11066.

Lukavsky, P.J., Kim, I., Otto, G.A. and Puglisi, J.D. (2003) *Nat. Struct. Biol.*, **10**, 1033–1038.

Madsen, J.C. and Sorensen, O.W. (1992) *J. Magn. Reson.*, **100**, 431–436.

Marino, J.P., Schwalbe, H. and Griesinger, C. (1999) *Accounts Chem. Res.*, **32**, 614–623.

Markley, J.L., Bax, A., Arata, Y., Hilbers, C.W., Kaptein, R., Sykes, B.D., Wright, P.E. and Wuthrich, K. (1998) *J. Biomol. NMR*, **12**, 1–23.

Masse, J.E., Bortmann, P., Dieckmann, T. and Feigon, J. (1998) *Nucl. Acids Res.*, **26**, 2618–2624.

McCoy, M.A. (1998) *J. Magn. Reson.*, **130**, 341–345.

Miclet, E., O'Neil-Cabello, E., Nikonowicz, E.P., Live, D. and Bax, A. (2003) *J. Am. Chem. Soc.*, **125**, 15740–15741.

Mollova, E.T., Hansen, M.R. and Pardi, A. (2000) *J. Am. Chem. Soc.*, **122**, 11561–11562.

Mooren, M.M.W., Wijmenga, S.S., Vandermarel, G.A., Vanboom, J.H. and Hilbers, C.W. (1994) *Nucl. Acids Res.*, **22**, 2658–2666.

Murray, L.J.W., Arendall, W.B., Richardson, D.C. and Richardson, J.S. (2003) *Proc. Natl. Acad. Sci. USA*, **100**, 13904–13909.

Nikonowicz, E.P., Sirr, A., Legault, P., Jucker, F.M., Baer, L.M. and Pardi, A. (1992) *Nucl. Acids Res.*, **20**, 4507–4513.

O'Neil-Cabello, E., Bryce, D.L., Nikonowicz, E.P. and Bax, A. (2004) *J. Am. Chem. Soc.*, **126**, 66–67.

Ono, A., Tate, S., Ishido, Y. and Kainosho, M. (1994) *J. Biomol. NMR*, **4**, 581–586.

Perez-Canadillas, J.M. and Varani, G. (2001) *Curr. Opin. Struct. Biol.*, **11**, 53–58.

Richter, C., Reif, B., Griesinger, C. and Schwalbe, H. (2000) *J. Am. Chem. Soc.*, **122**, 12728–12731.

Richter, C., Reif, B., Worner, K., Quant, S., Marino, J.P., Engels, J.W., Griesinger, C. and Schwalbe, H. (1998) *J. Biomol. NMR*, **12**, 223–230.

Sass, H.J., Musco, G., Stahl, S.J., Wingfield, P.T. and Grzesiek, S. (2000) *J. Biomol. NMR*, **18**, 303–309.

Shi, H.J. and Moore, P.B. (2000) *RNA*, **6**, 1091–1105.

Sibille, N., Pardi, A., Simorre, J.P. and Blackledge, M. (2001) *J. Am. Chem. Soc.*, **123**, 12135–12146.

Simorre, J.-P., Brutscher, B., Caffrey, M.S. and Marion, D. (1994) *J. Biomol. NMR*, **4**, 325–333.

Szyperski, T., Wider, G., Bushweller, J.H. and Wüthrich, K. (1993) *J. Am. Chem. Soc.*, **115**, 9307–9308.

Tjandra, N. and Bax, A. (1997) *Science*, **278**, 1111–1114.

Trantirek, L., Stefl, R., Masse, J.E., Feigon, J. and Sklenar, V. (2002) *J. Biomol. NMR*, **23**, 1–12.

Tycko, R., Blanco, F.J. and Ishii, Y. (2000) *J. Am. Chem. Soc.*, **122**, 9340–9341.

Warren, J.J. and Moore, P.B. (2001) *J. Biomol. NMR*, **20**, 311–323.

Wu, H.H., Yang, P.K., Butcher, S.E., Kang, S., Chanfreau, G. and Feigon, J. (2001a) *Embo J.*, **20**, 7240–7249.

Wu, Z., Delaglio, F., Tjandra, N., Zhurkin, V.B. and Bax, A. (2003) *J. Biomol. NMR*, **26**, 297–315.

Wu, Z.R., Tjandra, N. and Bax, A. (2001b) *J. Am. Chem. Soc.*, **123**, 3617–3618.

Zidek, L., Stefl, R. and Sklenar, V. (2001) *Curr. Opin. Struct. Biol.*, **11**, 275–281.

Zimmer, D.P. and Crothers, D.M. (1995) *Proc. Natl. Acad. Sci. U.S.A.*, **92**, 3091–3095.